Prespacetime Journal | March 2012 | Vol. 3 | Issue 3 | pp. 254-273
King, C., *Exploding the Dark Heart of Chaos: Part III*

254

Article

Exploding the Dark Heart of Chaos: Part III

Chris King[*]

Mathematics Department, University of Auckland

ABSTRACT

This paper, with its associated graphical software and movies, is an investigation of the universality of the cardioid at the centre of the cyclone of chaotic discrete dynamics, the quadratic 'heart' forming the main body of the classic Mandelbrot set. Using techniques investigating and exploring the continuity, bifurcations and explosions in its related Julia sets, we demonstrate its universality across a wide spread of analytic functions of a complex variable, extending from the classical quadratic, through higher polynomials and rational functions, to transcendental functions and their compositions. The approach leads to some interesting and provocative results, including decoding dendritic island periodicities, and multiple critical point analysis, leading to layered Mandelbrot set 'parameter planes', and intriguing issues of critical point sensitivity in the irregular structures in the Mariana trenches of the more complex functions. Part III of this article includes: 9. Getting to the Heart of the Riemann Zeta Function; Conclusion; Software and Demonstrations; Appendix 1: Combined Methods of Depicting Julia Sets and Parameter Planes; and Appendix 2: Ray Tracing Hypercomplex and Multi-dimensional Chaotic Iterations.

Key Words: chaos, cardioid, cyclone, Mandelbrot set, Julia set, bifurcation, analytic function.

9. Getting to the Heart of the Riemann Zeta Function

As an exercise in using these techniques at the frontier of functional complexity, and as a basis to generate open source code, I developed Matlab code to perform rapid calculation of the Riemann Zeta function:

$$\zeta(z) = \sum_{n=1}^{\infty} \frac{1}{n^z} = \prod_p \frac{1}{1 - p^{-z}} \quad [9.1]$$

on the entire complex plane, except the single pole at $z = 1$, using the Dirichlet Eta function $\eta(z)$, and the Lanczos approximation to the gamma function $\Gamma(s)$ to extend the domain to $\mathrm{Re}(z) < 0$:

$$\zeta(z) = \frac{\eta(z)}{\left(1 - 2^{1-z}\right)} = \frac{1}{\left(1 - 2^{1-z}\right)} \sum_{n=1}^{\infty} \frac{(-1)^{n-1}}{n^z}, \, \mathrm{Re}(z) > 0$$

$$\zeta(z) = 2\left(2\pi\right)^{-(1-z)} \cos\left(\frac{\pi(1-z)}{2}\right) \Gamma(1-z)\zeta(1-z), \, \mathrm{Re}(z) < 0 \quad [9.2]$$

A satisfactory alternative I have used subsequently is simply $\Gamma(z) = \frac{1}{z} \prod_{k=1}^{\infty} \frac{(1 + 1/k)^z}{1 + z/k}$

The Lanczos approximation is defined as follows:

[*] Correspondence: Chris King http://www.dhushara.com E-Mail: chris@sexualparadox.org
Note: This work was completed 8th March – 22nd April 2009.

$$\Gamma(z+1) = \sqrt{2\pi}\left(z+g+\frac{1}{2}\right)^{z+\frac{1}{2}} e^{-\left(z+g+\frac{1}{2}\right)} A_g(z), \quad \Gamma(1-z)\Gamma(z) = \frac{\pi}{Sin\pi z}, \ \mathrm{Re}(z) < 0$$

[9.3]

$$A_g(z) = \frac{1}{2}p_0(g) + p_1(g)\frac{z}{z+1} + p_2(g)\frac{z(z-1)}{(z+1)(z+2)} + \mathsf{K} \quad g: \mathrm{Re}\left(z+g+\frac{1}{2}\right) > 0$$

with $g = 9$ and $p_i(g)$ calculated independently by Paul Godfrey as constants from the relation:

$$p_k(g) = \sum_{a=0}^{k} C(2k+1, 2a+1)\frac{\sqrt{2}}{\pi}\left(a-\frac{1}{2}\right)!\left(a+g+\frac{1}{2}\right)^{-\left(a+\frac{1}{2}\right)} e^{a+g+\frac{1}{2}}$$

where
$$C(1,1) = C(2,2) = 1, \ C(i,1) = -C(i-2,1)$$
$$C(i,i) = 2C(i-1,i-1), \ C(i,j) = 2C(i-1,j-1) - C(i-2,j), \ i > j$$
are coefficients of the
Chebyshev polynomial matrix.
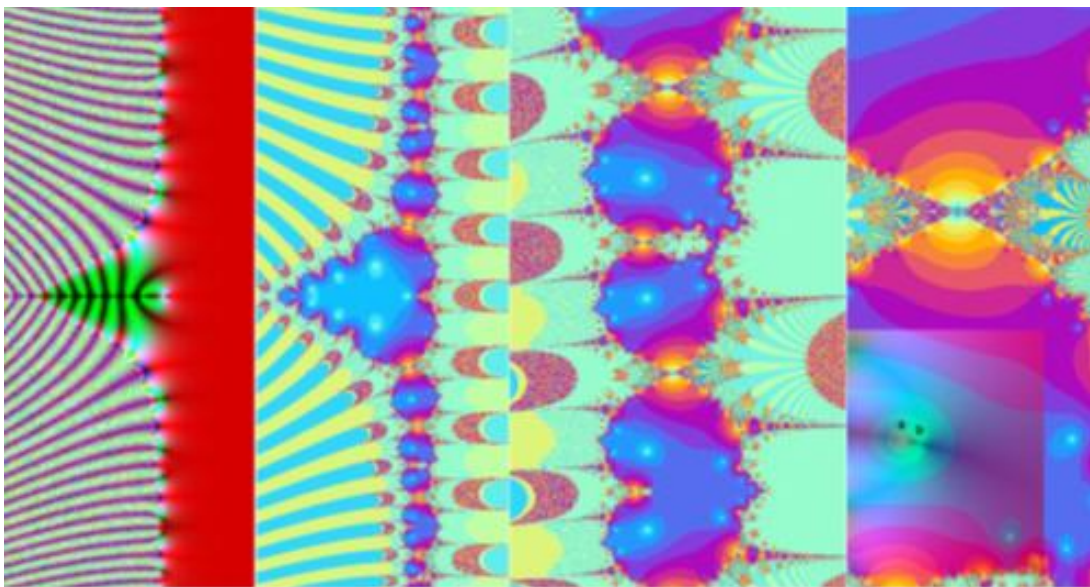
Fig 37: (a) The Riemann Zeta function $\zeta(z)$, showing its pole at 1 the trivial zeros at even negative real values and the non-trivial zeros on the line x=1/2. (b) The Julia set of $\zeta(z)$, highlighting eventually fixed points in the internal basin mapping to $\alpha =\sim -0.2959$, to which the zeros are also mapped. Inset in right overlap of eventually fixed point and non-trivial zero (a, b) showing their proximity, with the eventually fixed point to α lying on the curve where $\mathrm{Im}(\zeta(z)) = 0$.

The iteration takes the first 2001 terms of $\eta(z)$ and halves the next term to average contributions near 0, where the terms remain large. The overall process is computationally extremely intensive and the self-organized criticality of $\zeta(z)$, launching the positive half-plane to the neighbourhood of the pole at 1, is liable to stress numerical calculation to the limit. However the results are intriguing and provide support for the dark heart of the parameter plane even under these extreme circumstances. As illustrated in fig 37, the Julia set of $\zeta(z)$ (Woon) forms the boundary between the basin of attraction of ∞ and the attracting fixed point $\alpha = -0.2959050055752$. The first six non-trivial zeros of the function, from $\beta = 0.5 + 14.1347i$ on, famous for the Riemann hypothesis - that they are on all on the line $x=1/2$ - lie in the basin of attraction of this fixed point. In fact all the zeros of the function do, including the trivial ones at $z = -2n$, as all are mapped to 0, which iterates to α.

The overwhelming reason for the zeros to be on the line $x = \frac{1}{2}$ is that there is an internal symmetry in the analytic extension of the function to $\square - \{1\}$, which was expressed by Riemann (1859), in the form of the reflection relation around $x = \frac{1}{2}$:

$$\Gamma\left(\frac{s}{2}\right)\pi^{-\frac{s}{2}}\zeta(s) = \Gamma\left(\frac{1-s}{2}\right)\pi^{-\frac{1-s}{2}}\zeta(1-s) \text{ [9.4].}$$
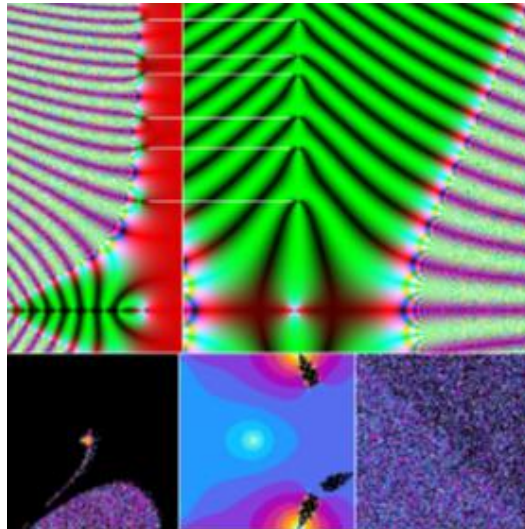
Fig 38: Above: The functions ζ, ξ have the same set of non-trivial zeros but the latter also displays the internal symmetry about the roots. (Lower Left) Island iterating to α around -20 shows the Julia set contains disconnected components. (Centre) Region around -16 is in the main internal basin. (Right) Region around 8 in the divergent basin, shows critical behavior probably resulting from computational numerical overflow at the pole.

Once expressed by Riemann in the form $\xi(t) = \Gamma\left(\frac{s}{2}\right)(s-1)\pi^{-\frac{s}{2}}\zeta(s), \ s = \frac{1}{2} + it$ [9.5], this internal symmetry is made evident, as shown in fig 38, comparing ζ, ξ. It is also evident in the reflective dynamics of the iteration around the Julia set of $\zeta(s)$ in fig 37. The zeros are definitely confined to the critical strip $x = [0,1]$, as x cannot be greater than 1 by the Euler product formula [9.1], whose individual terms immediately result in prime sieving of the series formula, when taken to the left hand side, and x cannot either be less than 0 as a result of the reflection formula.
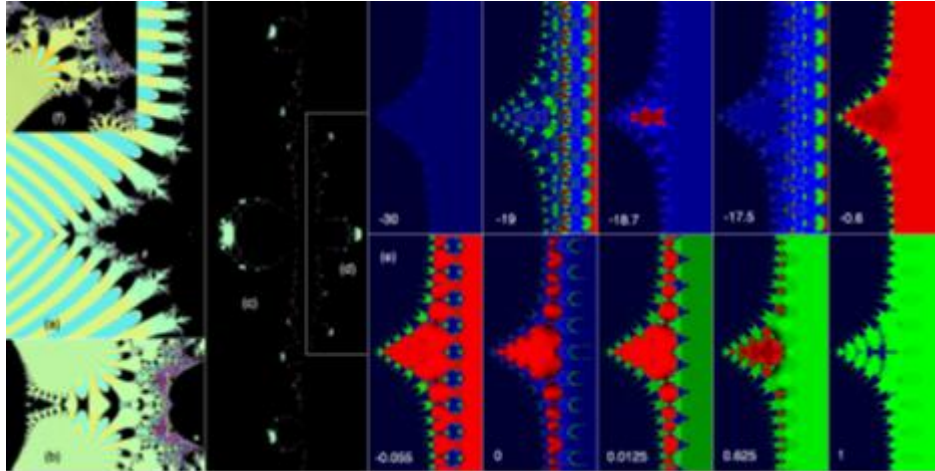
Fig 39: (a) Parameter plane of $\zeta_c(z) = \zeta(z) + c$ iterating from the critical value 1 real [-40,6] imaginary [-40,40]. (b) Enlarged region [-20.5,-15.5] showing complex bifurcations. (c) A tiny fractal 'lake' barely visible around $c = 0$, shown expanded real [-0.1,1] imaginary [-1.1]. This corresponds to c for which the positive half-plane diverges due to the pole at 1. Inset in (c) at half the scale of (b) is the corresponding 'lake' iterating from 0 corresponding to c for which the zeros of $\zeta(z)$ diverge. (d) Sample Julia sets on the real line, with colour chosen to distinguish divergence, convergence to the critical strip and convergence into positive half plane - shades of blue for points tending to ∞, red for points asymptotic to a periodicity in the critical range, green asymptotic to a periodicity with real parts entirely positive, or including a periodic value greater than 10, and grey to black for non-periodic points (largely absent). The range from -15 to -0.1 is similar to 0.6 with no apparent bifurcations. (f) Inset of region marked by # in (a).

Although the Julia set appears to be connected, this is unlikely, because all the trivial zeros on the negative real axis also iterate to the attracting fixed point and the dappled lacunae in the divergent basins are in a state of self-organized criticality, where divergent values and values convergent to α appear to densely interpenetrate, as emphasized in fig 38 where diverging points are black and those converging to α are coloured. This is likely to be a result of computational overflow at the pole and indeed testing values with Matlab's own standard zeta function (presumably derived from the Maple engine as it is in the symbolic toolbox) froze the computation after three iterations.

To test the question of parameter planes as a measure of the bifurcations of a family of Julia sets, we now examine the parameter planes of the function $\zeta_c(z) = \zeta(z) + c$. The most outstanding critical value of $\zeta(z)$ is the value 1, to which all z with positive real values tend as $\mathrm{Re}(z) \to \infty$. This however is a case of self-organized criticality, as it projects the entire positive half plane directly on to the neighbourhood of the pole at 1. The Julia set $J_c(\zeta)$ is thus extremely sensitive to small changes in c, undergoing explosions of the positive half-plane for c as small as 0.001.

In fig 39 we show the parameter plane for the critical value 1, in which the black regions indicate the critical value remains finite and colours indicate divergent iteration to ∞, along with corresponding illustrations of Julia sets, which highlight both complex bifurcations on the real line in the interval [-21,-15], and explosions of the positive half plane on either side of 0, at ~-0.005 and ~0.001. Both these features correspond closely to the parameter plane, which shows both complex fractal structure in the former range and a tiny fractal 'lake' around 0 connected by a dendritic thread of further 'lakes' winding in the imaginary direction to the divergent region.

A second parameter plane iterating from the value 0, which, although it is not strictly a critical value is the value of all the zeros of $\zeta(z)$. This provides a similar characteristic in the range -21-15 and a fractal 'lake' centered on 1, corresponding to the bifurcations as the zeros cross the pole at 1 and escape the internal basins of the Julia set, which has already become disconnected into an infinite set of connected islands.
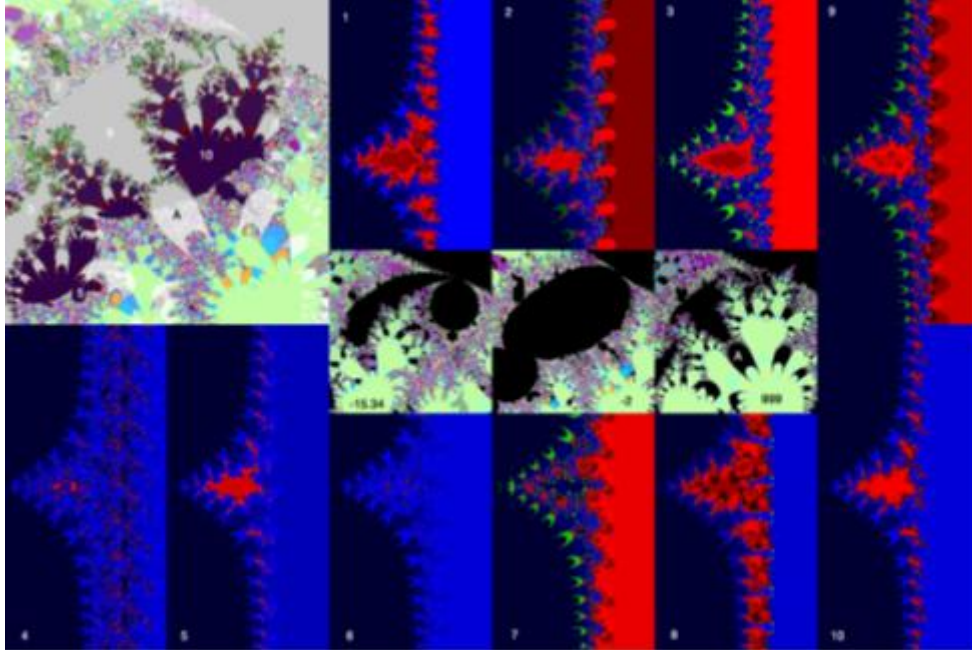
Fig 40: Examination of the region [-16,-15]x[-1,-2], marked * in fig 39, shows the role of the parameter planes on the 'critical' values 0 (taken by iterating from the zero -2) and 1 (taken by iterating from 999) classify the Julia sets of $\zeta_c(z)$. For comparison the critical saddle at ~ -15.34 with critical value 0.5206 is also plotted in this domain displaying a classic period multiplying bulb. In the centre are shown the local parameter planes for these three values. Top left: The two parameter planes overlapped to show unions and intersection with locations of Julia set parameters 1 – 10 (A is an artifact). Only 0 and 1 show classifying attributes, with c values in M_0 displaying connected central regions (red) containing the attracting fixed point for the zeros. By contrast, c values in M_1 display bounded periodicities in the positiveve half-plane (here red). Values of c in both sets display both features, those in one, one , and those in neither, neither, confirming the classification.

Conclusion:

The approach gives a complete investigative approach to confirming the universality of the Mandelbrot 'dark heart of chaos' across the very broad class of complex functions possessing polynomial-type critical points. The paper has demonstrated that multiple critical point analysis, as developed to deal with cubics and higher polynomials extends readily to composite transcendental functions and thus embraces the comprehensive majority of complex functions central to mathematics. The ultimate conclusion is that chaos, represented by the Julia sets, or their bifurcation kernels will always trap the critical points of the function as the last super-stable points of escape into basins of attraction if these kernels are locally homeomorphic to connected sets.

Software and Demonstrations:

The software used to investigate this was an intel native Mac OSX XCode application-generating project originally developed as a Mandelbrot explorer for the standard quadratic by Michael C. Thornburgh and converted to a generalized Mandelbrot/Julia function explorer by the author. A Metrowerks C program suite developed by the author was used to generate movies and Julia sequences at specific loci. The software, source code and movie demonstrations is available from a link at http://www.dhushara.com.

All of the viewers work by dragging a rectangle to kexpand a sub-region. If you click you will switch between the parameter plane and the Julia set of that coordinate. Sometimes checking the random box will fill the interior basins. The Herman viewer toggles from a-Mandelbrot to a c-Mandelbrot with the chosen a and then to the ac-Julia set. Reset takes you back to the beginning. The number of threads accelerates the program at the expense of other threaded programs. Increasing the number of iterations gives a slower, but more accurate image.

1. Compiled viewers of each of the examples
2. Source Code of: Layered Cubic, 2-parameter Herman, Illuminated Cosine, Sinz+Sin2z/2, Cosz+Cos2z, Layered Sinz/z
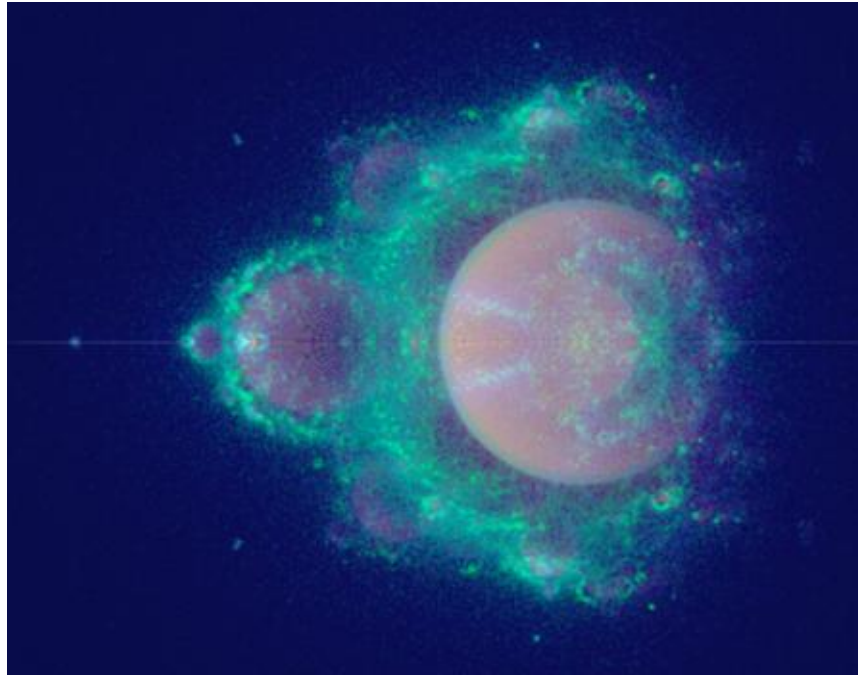
Fig 41: Ghostly 'Buddhabrot' image plots the collective orbits of the critical point of $f(z) = z^2 + c$ by adding 1 to each pixel that the orbit from the critical point of each c value on the plane visits. The orbits of c points outside M are iterated in cyan overlying the orbits of c points in M iterated in shades of ochre and magenta.

Appendix 1: Combined Methods of Depicting Julia Sets and Parameter Planes

Level Set Method LSM

Begin with the point $z_0 = (x, y)$ for a fixed c and iterate $z_{n+1} = f_c(z_n) + c$. If we are depicting the Mandelbrot parameter plane, we begin instead with the critical point $z = 0$ and iterate for each $c = (x, y)$. If the point escapes a circle say of radius 10, $|z_n| < M$, we colour it by the number of iterations. If it remains bounded after a fixed number of iterations, we assume it cannot escape and colour it black (or white in the above examples).

This method will work for the Julia set of any function provided we can determine basins of attraction of fixed or periodic points, to apply the algorithm to. In the case of $f_c(z) = z^2 + c$ this is ∞ and the Julia set is the boundary of the basin of attraction of ∞. In other functions it may be finite and multiple. In the case of transcendental functions, such as cos and exp, ∞ is an essential singularity and the Julia set is the closure of its basin of attraction and the target set may be $|imag(z_n)| < M$ or $|real(z_n)| < M$. The method will also work for the parameter plane (Mandelbrot set) of any function provided we can locate and handle the critical points and establish individual parameter planes for each.
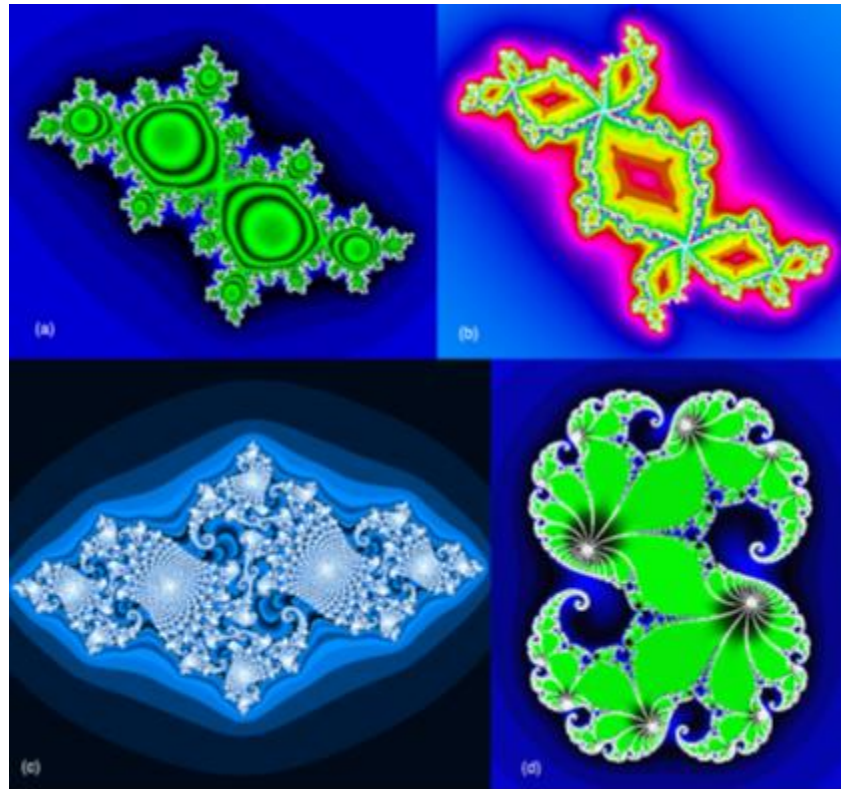
Fig 42: Quadratic Julia sets depicted by combined methods. (a) A Siegel disc ($c = \dfrac{e^{i\theta}}{2} - \dfrac{e^{2i\theta}}{4}$, $\theta = \pi(-1 + \sqrt{5})$).

Exterior (blue) by level set, Julia (white) by modified inverse iteration, irrational flow (green) by the sine of the velocity.

(b) Super-attracting period 3 (Solution of $(c^2 + c)^2 + c = 0$). Exterior by continuous potential, Julia by modified inverse iteration, interior basins by level set. (c) Seahorse valley dendrite ($c = -.74543 + .11301i$) by distance estimator, exterior by level set. (d) Parabolic bifurcation period1 to 20 ($c = .27334 + .00742i$ adjacent to

$c = \dfrac{e^{i\theta}}{2} - \dfrac{e^{2i\theta}}{4}$, $\theta = \dfrac{2\pi}{20}$). Exterior by level set, Julia by modified inverse iteration, petals by velocity.

Variation 1 Internal Basins:

If the Julia set has an internal attracting periodic point we can test for this by also finding the periodic cycle by first iterating the critical point until it becomes within δ of being periodic and then colour a non-escaping point by the number of iterations to bring $z_0 = (x, y)$ within δ of a point on the cycle.

Variation 2 Continuous Potential (Quadratics only):

We can derive a continuous potential with an even gradation but less sensitivity at the boundary of J_c by

using the continuous potential formula $P = \dfrac{\log|z_n|}{2^n}$ for an escaping point.
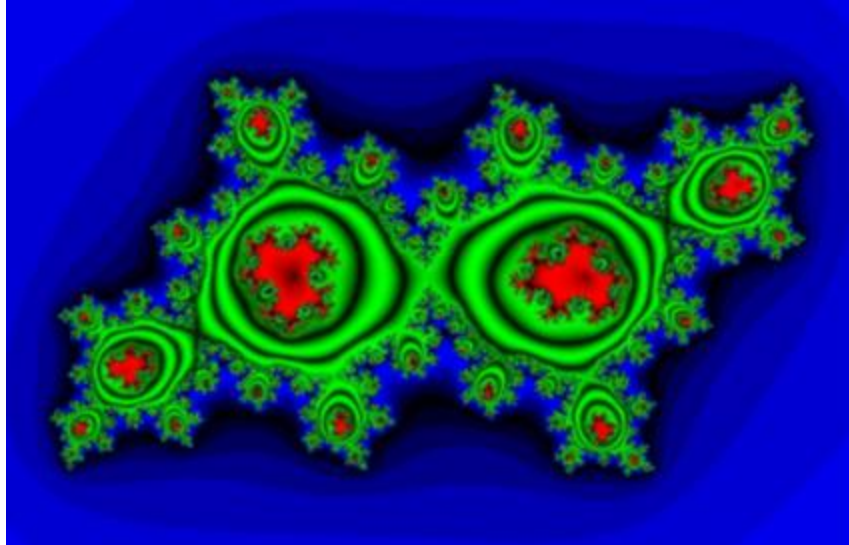
Fig 43: Herman ring $f(z) = (-1 + \sqrt{5})\pi z^2 \dfrac{z-4}{1-4z}$ Irrational annular flow depicted
by sine of the discrete velocity, interior basin level sets red, exterior blue.

Variation 3 Distance Estimator (Quadratics only)**:**

For dealing with dendritic Julia sets, or the Mandelbrot set, to demonstrate connectivity, we can make two additional tests to detect proximity to J_c :

(a) Test for overflow of the derivative of any point on the escaping orbit: $|z'_i| > O$

(b) Test for distance $dist = 2\dfrac{|z_n|}{|z'_n|}\log|z_n| < \delta$

We can calculate orbit derivatives iteratively as follows $z'_{i+1} = z_i z'_i,\ z'_0 = 1$ for the Julia set and $z'_{i+1} = z_i z'_i + 1,\ z'_0 = 0$ for the Mandelbrot set, since we are differentiating with respect to c rather than z. In practice, $O \sim 1600000$, $\delta \sim 0.1$. The derivative overflow tests for highly repulsive dynamics adjacent to J_c .

Variation 4 Discrete Velocity of non-attracting Basins and Petals:
Compute, for the points that don't escape, the average discrete velocity $|z_{i+1} - z_i|$ on the orbit.

Variation 5 Binary Decomposition: Split the level sets light or dark depending on whether the n-th iterate is in the upper or lower half plane - i.e. has imaginary part positive or negative. This highlights both equipotential level curves and sections of external rays. See fig 5.

Variation 6: Pickover Stalks: Choose a target neighbourhood, e.g. narrow stalks along the x and y axes, or circles at the origin. Iterate a point using the level set method, but if it enters the target region, colour it with the minimum number of steps to enter the target instead.
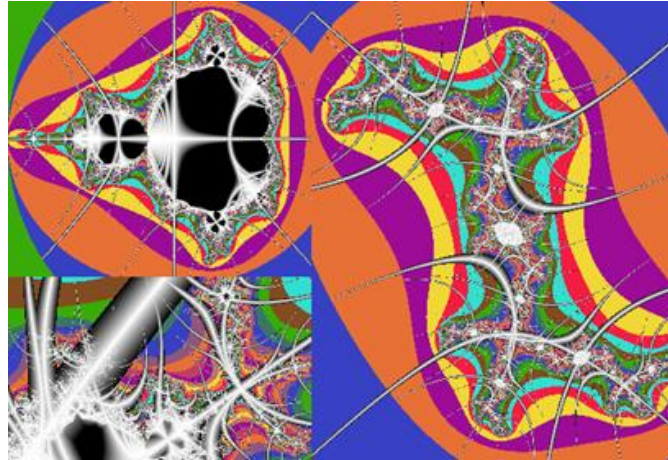
Fig 43(b) Pickover stalks emerging from the Julia set asterisked lower left

Inverse Iteration Method IIM

First find a repelling fixed point , u_0 , by solving $f_c(z) = z$. For $f_c(z) = z^2 + c$, one of the two fixed points

$z = \dfrac{1 \pm \sqrt{1-4c}}{2}$ is always a repeller as $\left| f_c'(z) \right| = 2z = 1 \pm \sqrt{1-4c}$, unless $c = \dfrac{1}{4}$. Now plot the two

inverse images $z_i = \pm\sqrt{z_{i+1} - c}$ of this point and repeat to form the 2^n n-th inverse iterates. This method requires a heap, or some equivalent data structure, to keep track of the branching tree of inverse iterates. If memory is exceeded we can randomly plot one or other roots and its pre-images. However this method has the problem that it is computationally intractable because the points are exponentially unevenly distributed over the Julia set, due to multifractality (fractal redistribution of the probabilities), resulting in the inverse mapping being strongly contractive to some features leaving others unrepresented, and thus fails to represent significant features of J_c , even with exhaustive computation times.

Variation 1 Modified Inverse Iteration MIIM (see figs 3, 13b):

We cut off the sub tree from a given $u_{m_k} : f_c^{(k)}(u_{m_k}) = u_0$ if the derivative $\left| (f_c^{(k)})'(u_{m_k}) \right| > M$. This eliminates dominant highly contractive regions of the inverse iteration, which have already been registered. We can calculate successive derivatives iteratively $\left| f_c'(u_{m_{i+1}}) \right| = 2\left| u_{m_i} \right| \left| f_c'(u_{m_i}) \right|$.
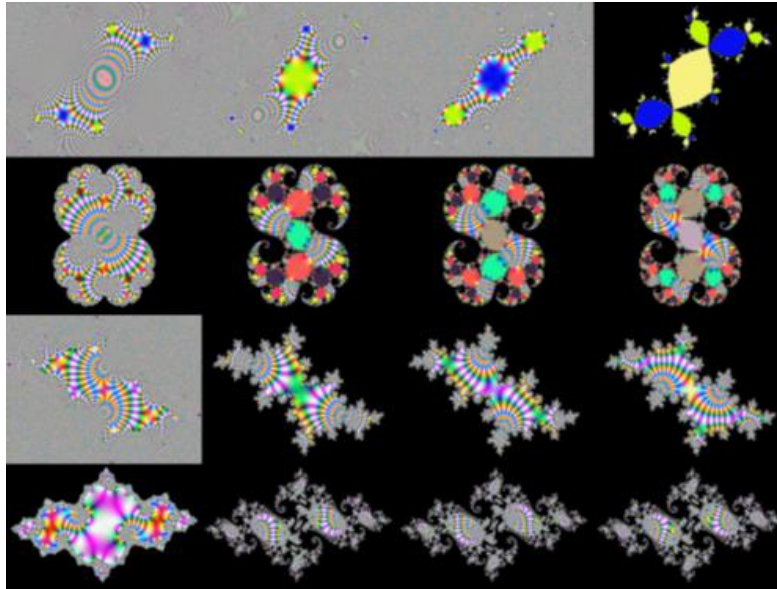
Fig 44: Wave function method developed during the production of this work portrays the dynamics leading to formation of Julia sets by iterating successive compositions of f(z) with the complex wave function illustrated by colouring the plane shades of red (r) and green (g) according to a conformal function, such as

$$w(z) = \cos(kr\,\mathrm{real}(z)) + i\sin(kg\,\mathrm{imag}(z)) \text{ or } w(z) = \cos(kr|z - crit|) + i\sin(kg\arg(z - crit))$$ which highlights recursive pre-images of the critical point.

Conformal Wave Function Method

This method developed during production of this paper to gives a dynamic picture of the action of iteration of complex functions having two input and two output variables. A suitable function (see fig 45) is used to generate conformal interfering waves of oscillating colour, forming a Cartesian or polar grid. Successive iterates of $f(z)$ are then applied to form a sequence of images $w(f^n(z))$, with numbers which have exceeded computational bounds assigned black by default (Matlab does this automatically). The method generates a discrete dynamical movie of the recursive action of f on the plane, showing how the repeated application of f leads to formation of a Julia set, highlighting the internal dynamics of the basins, including attracting and neutral mode-locked periodic points, irrational flows and Cantor processes. The process is a form of inverse iteration since the n-th frame is drawing the n-th pre-image of the domain of the wave function. If polar coordinates about the critical point are used, this highlights pre-images of the critical point.
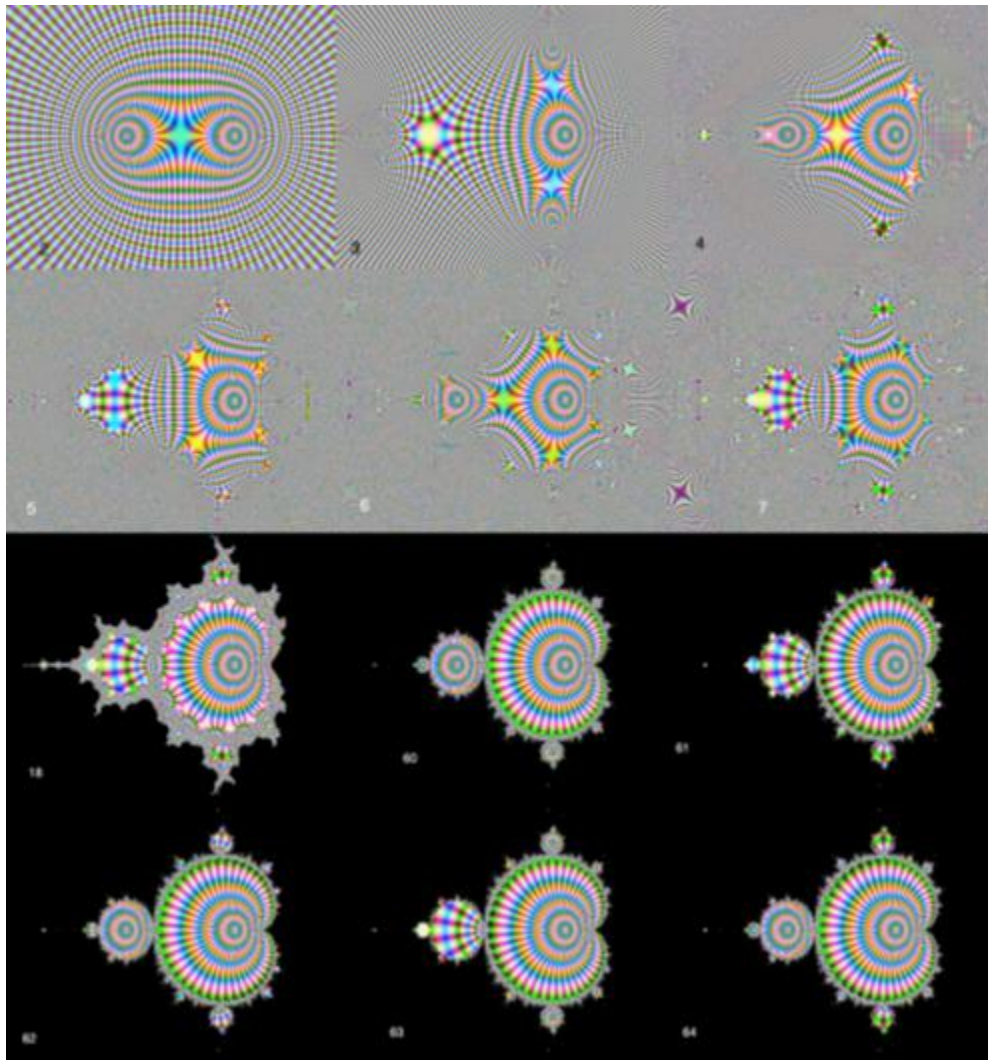
Fig 45: Wave function method highlights the dynamic periodicities of all regions of the parameter plane. The first frames immediately highlight periodicities of the critical point as images of the origin, showing both locations and periodicities of period 2 to 7 super-attracting bulbs and dendritic islands. Later iterations highlight the periodicities of the period 2, 3, 4, and 5 bulbs starting with frame 60 having all these bulbs showing images of the origin.

One can also produce a dynamic movie of the internal periodicities on the Mandelbrot set by repeatedly inserting the original c value into each iterate of f, expressed in terms of the critical value. For $f(z) = z^2 + c$ this is just c, but for $f(z) = cz(1-z)$, with critical number ½ and critical value $v = c/4$, we need to insert $4v$, and use a wave function centered on the v value which will fix the critical point, i.e. $v = $½ or $c = 2$.

Chaotic Processes and Discrete Iteration

All computer methods suffer from numerical over/underflow and the incapacity of any simulation to accurately approximate a dynamical process, which is sensitive to its initial conditions. Thus Mandelbrot originally thought 'his' set was disconnected into islands until Douady and Hubbard's, conformal proof of its connectedness demonstrated the contrary. However these problems can lead to intriguing issues of computational complexity.
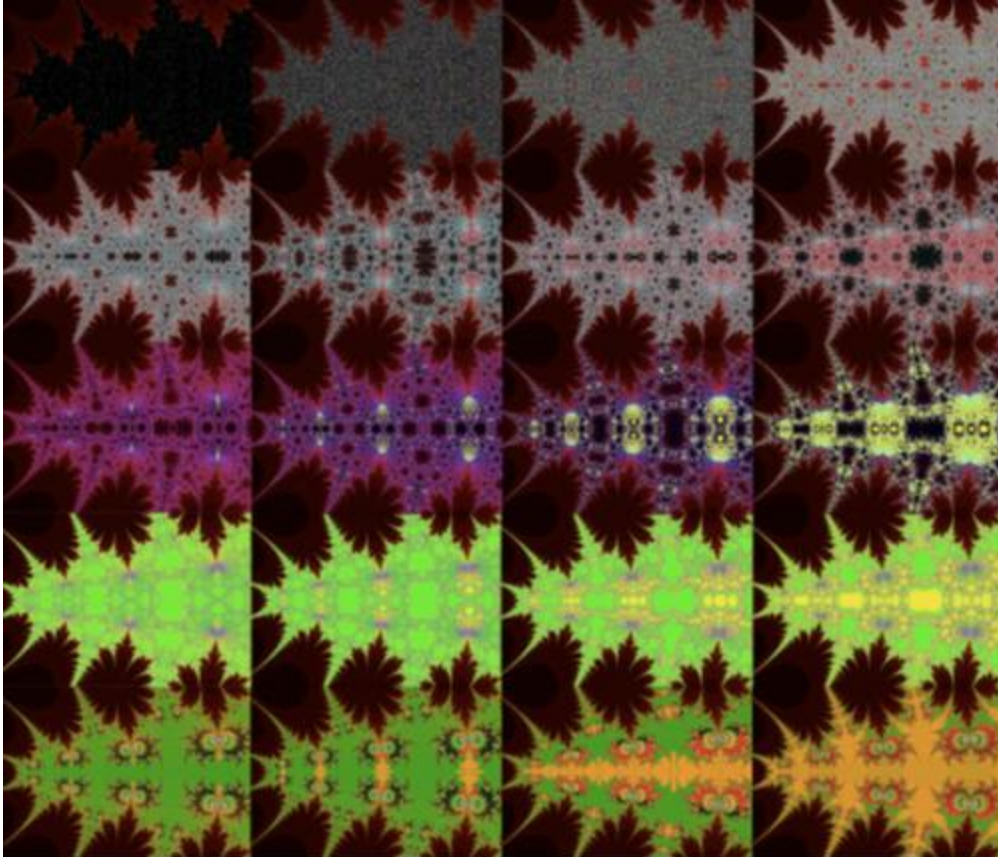
Fig 46: Cosine root principal explosion in 16384 iterations to show the initial stages of the explosion, using the arctan formula. As can be seen, in contrast to fig 29, the initial explosion is characterized as an atomic cosmological 'big-bang' filling parabolic space with extremely high iteration number structures at the limits of complexity resolution, followed by successively slower explosion waves of successively simpler level set structure, as the process progresses. These suggest associations both with quantum chaos and with cellular automata, some of which, on the 'edge of chaos' in discrete system terms, can act as universal computers.

The function $f(z) = \cos(\sqrt{z})$ shows how sensitive computer processes can be to underflow and overflow, resulting in discrete artifacts similar to a cellular automaton, which can be even more beautiful and complex than the underlying process. The underlying degree of the function is 1, since the first order degree of the cosine 2 is cancelled by the degree ½ of the root in composition. The process thus becomes highly sensitive to floating point over/underflow at bifurcation points, particularly the principal explosion point. A hint of why the phenomena of fig 46 may be happening can be seen from fig 47, where discrete effects emerge from the underflow of computations of a radial wave function under recursive dilation of the origin.

In taking $\sqrt{z}$, we can proceed in several ways. In fig 46 we have used $\sqrt{re^{i\theta}} = \sqrt{r}e^{i\theta/2}$ the apparently simplest route. However this involves both calculating a double square root $\sqrt{r} = \sqrt{\sqrt{x^2 + y^2}}$ and using the transcendental arctan to halve the angle $\dfrac{\theta}{2} = \dfrac{1}{2}\tan^{-1}\dfrac{y}{x} + k\pi,\ k = 0,1$ making allowance for singularities.

Alternatively, we can proceed directly:

$$(a+ib)^2 = z = x+iy,\ a^2 - b^2 = x,\ 2ab = y,\ b = \frac{y}{2a},\ a^2 - \frac{y^2}{4a^2} = x,$$

$$(2a^2)^2 - 2x(2a^2) - y^2 = 0,\ 2a^2 = \frac{2x \pm \sqrt{4x^2 + 4y^2}}{2},\ a = \frac{\sqrt{x + \sqrt{x^2 + y^2}}}{\sqrt{2}}$$

At this point we would be tempted to use $b = \frac{y}{2a}$, but this is liable to over/underflow error and singularity, resulting in gross divergence at the explosion point. Instead we can define:

$$a = \frac{y}{2b},\ \frac{y^2}{4b^2} - b^2 = x,\ (2b^2)^2 + 2x(2b^2) - y^2 = 0,\ 2b^2 = \frac{-2x \pm \sqrt{4x^2 + 4y^2}}{2},\ b = \frac{\sqrt{-x + \sqrt{x^2 + y^2}}}{\sqrt{2}}$$

This method gives the series of images in fig 33 which coincide with those for the other functions.
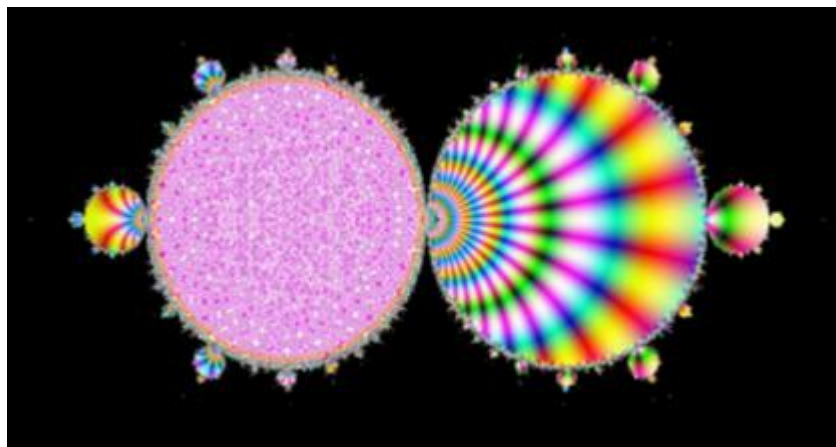
Fig 47: Super-attracting basin of $f(z) = cz(1-z)$ becomes a Moire pattern when a radial wave function about the origin is used, as the inverse process is recursively dilating the origin.

Appendix 2: Ray Tracing Hypercomplex and Multi-dimensional Chaotic Iterations

We now investigate how Julia and Mandelbrot sets of the 4D Quaternions, bicomplex numbers and other systems, such as the spherical polar Mandelbulb iteration can be investigated in 3D space.

Quaternionic and Hypercomplex Systems

The quaternions *Q* are defined as:
$$Q = \{z = a + bi + cj + dk,\ i^2 = j^2 = k^2 = -1,\ ij = -ji = k,\ jk = -kj = i,\ ki = -ik = j\}$$
Since *i*, *j*, *k* share a symmetrical relationship, a pure unit quaternion *u* = (0, *b*, *c*, *d*) behaves as a rotation in 3D space $\Box^3$, with each of *i*, *j*, *k* corresponding to rotations of 180 about the axes.

This symmetrical representation can be extended to 1+*n* dimensions, resulting in so-called hypercomplex systems (Dang et. al.). One needs to note however that the only true division rings over the reals where elements can be both multiplied and divided and give rise to a full suite of rational and transcendental functions are the complex numbers $\Box$ and quaternions Q^4 , with a non-associative extension to the octonians *O*, by effective quaternion 'complexification'.

Note that in the quaternions, De Moivre's theorem still holds when we express a given element in terms of a pure quaternion unit vector $z = a + bu = r\cos(\theta) + ur\sin(\theta),\ z^n = r^n\big(\cos(n\theta) + u\sin(n\theta)\big)$, but the

loss of commutativity means that, for example $zpz \neq pz^2$, so there is no unique way to write a poynomial in terms of powers of *z*, however, like $\Box$, we can develop transcendental functions such as the log and exp.
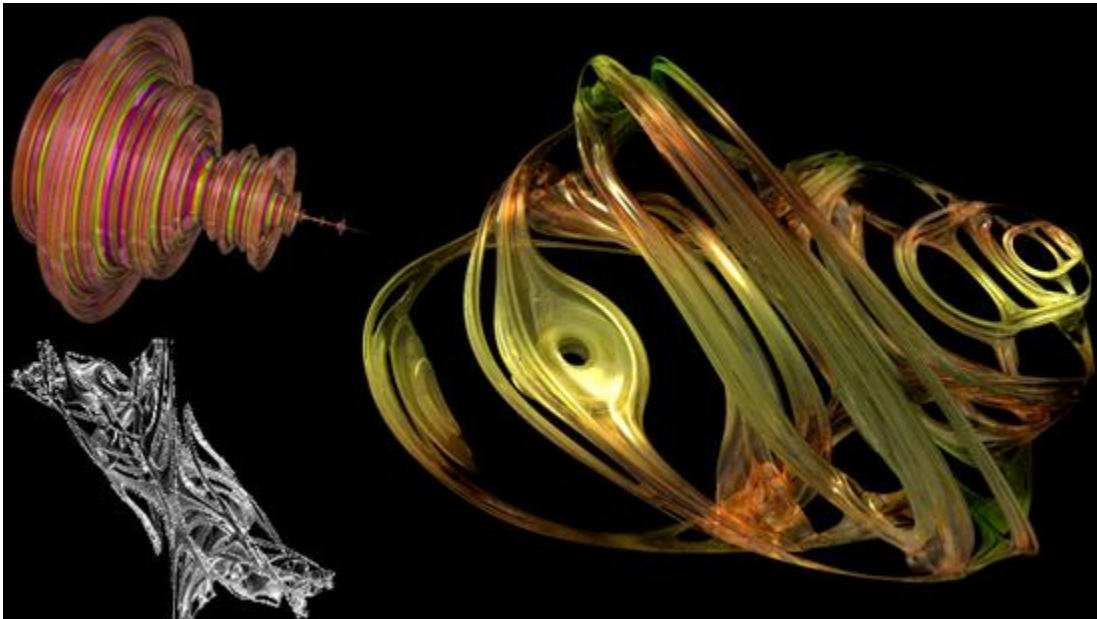
Fig 48: (Top left) Quarternionic Mandelbrot set in 3D is a solid of revolution of the complex 2D Mandelbrot set about the real axis. (Right): Quaternionic Julia set projected into $\Box^3$. (Lower left) Symmetric projection. A given Julia set of $f(z) = z^2 + q, \ q \in Q$ can be represented in 3D because it can be rotated by an angle θ in parameter space to a related Julia set $f(z) = z^2 + c, \ c \in \pounds, \ z \in Q$. The coordinates (R, I, θ) can be used to define a Julia set of an arbitrary via the rotated mapping $f_\theta(z) = e^{-i\theta}z^2 + e^{i\theta}c, \ z \in Q, \ c = R + iI \in \pounds$.

If we are considering a quadratic mapping in *H*, we have:

$$z^2 = (a + bi + cj + dk)^2 = a^2 - (b^2 + c^2 + d^2) + 2abi + 2acj + 2adk$$

Hence, given the iteration $f(z) = z^2 + c$, we have the following four-assignments:

$$a \leftarrow a^2 - (b^2 + c^2 + d^2) + c_r, \ b \leftarrow 2ab + c_i, \ c \leftarrow 2ac + c_j, \ d, \leftarrow 2ad + c_k$$

Expressed in terms of vectors, for a level set, or escape-time algorithm, this becomes:

$$a \leftarrow a^2 - |\mathbf{r}|^2 + c_r, \ \mathbf{r} \leftarrow 2a\mathbf{r} + \mathbf{c}, \ a^2 + \mathbf{r}^2 < \text{'bailout'}.$$

Now an apparent paradox arises, in which the Mandelbrot set appears 'simpler' than the Julia set, in the sense that it can be fully represented in a lower dimensional space.

If we are considering the Mandelbrot iteration $0 \to c \to c^2 + c \to \ldots$ then **r** and **c** are co-directional. If **c** is written as $c = c_r + |\mathbf{c}|u, \ \text{u} = \dfrac{\mathbf{r}}{|\mathbf{r}|}$ then $u^2 = -1$ and the iteration preserves the complex plane containing the real axis and the axis of *u*. The quaternionic Mandelbrot set thus consists of a complex 2D Mandelbrot set rotated about the real axis to form a spherically symmetrical set in *Q*. This can be represented in $\Box^3$ as a rotation of the 2D complex Mandelbrot set about the real axis, as shown in fig 1(a).

The same situation pertains for a Julia set $f(z) = z^2 + r,\ r \in \degree,\ z \in Q$.

Now let us consider an iteration of the form $f(z) = c_1 z^2 + c_2,\ c_1, c_2 \in \pounds$. It turns out that the dynamics of this iteration are independent of the angle ϕ in $z = z_1 + e^{i\phi} z_2,\ z_1, z_2 \in \pounds$.

Let $z = (a, b, c, d) \in Q$ then $z = (a + bi) + (c + di)j = z_1 + z_2 j,\ z_1, z_2 \in \pounds$.

Now consider $g_\phi(z) = a + bi + e^{i\phi}(cj + dk)$. If we choose ϕ so that $e^{-i\phi} = \dfrac{\bar{z}_2}{|z_2|}$, then

$$g_{-\phi}(z) = z_1 + e^{-i\phi} j z_2 = z_1 + \frac{\bar{z}_2 z_2}{|z_2|} j = z_1 + |z_2| j = a + bi + |z_2| j \in \degree^3.$$

If $f(z)$ is as above then $g_\phi(f(g_{-\phi}(z))) = f(z)$, so the rotated dynamic is the same as the original.

Now let us consider $f_q(z) = z^2 + q,\ q, z \in Q$. Given q there exists $p \in Q : |p| = 1,\ c \in \pounds : pqp^{-1} = c$. The Julia set $J_q = pJ_c p^{-1}$ simply a rotation of the dynamic in Q^4 to $f_c(z) = z^2 + c,\ z \in Q,\ c \in \pounds$.

The effect of the function $f_{\theta,c}(z) = e^{-i\theta} z^2 + e^{i\theta} c,\ z \in Q,\ c = R + iI \in \pounds$, is to simply rotate the Julia set of the iteration $f(z) = z^2 + c,\ c \in \pounds$ unchanged within $\square$, but resulting in very different Julia sets in the expansion to the rest of Q^4. It is thus common to investigate the triple (R, I, θ) and iterate the above function $f_{\theta,c}(z)$ in Q^4, projecting the resulting points (z, z_i, z_j, z_k) to $(z, z_i, z_j) \in \degree^3$ to give 3D projections of a representative spectrum of quaternionic Julia sets.

Quaternionic versions of transcendental and other functions can be defined and portrayed using the above methods, according to the following definitions (Halayka 2009):

$$
\begin{aligned}
t &= Z_x, \\
\vec{V} &= Z_y,\ Z_z,\ Z_w, \\
|\vec{V}| &= \sqrt{Z_y^2 + Z_z^2 + Z_w^2}, \\
\text{norm}(Z) &= |Z|^2 = t^2 + \vec{V} \cdot \vec{V}, \\
\text{inv}(Z) &= t/\text{norm}(Z),\quad -\vec{V}/\text{norm}(Z), \\
\sin Z &= \sin t \cosh |\vec{V}|,\quad \cos t \sinh |\vec{V}|\vec{V}/|\vec{V}|, \\
\cos Z &= \cos t \cosh |\vec{V}|,\quad -\sin t \sinh |\vec{V}|\vec{V}/|\vec{V}|, \\
\exp Z &= \exp t \cos |\vec{V}|,\quad \exp t \sin |\vec{V}|\vec{V}/|\vec{V}|, \\
\sinh Z &= \sinh t \cos |\vec{V}|,\quad \cosh t \sin |\vec{V}|\vec{V}/|\vec{V}|, \\
\cosh Z &= \cosh t \cos |\vec{V}|,\quad \sinh t \sin |\vec{V}|\vec{V}/|\vec{V}|.
\end{aligned}
$$

Octonionic Julia Sets (Griffin and Joshi 1992) and a generalized Mandelbrot set (Griffin and Joshi 1993) can also be defined and portrayed, and display new features associated with their non-associativity, in which $(ij)l = -i(jl) \neq i(jl)$.

These can either be portrayed by inverse iteration, or by using a distance estimator and 3D ray tracing to reflect right rays from a source off a tangent plane determined by a normal from a point estimated iteratively to be arbitrarily close to the Julia set using an iterative process similar to that used to generate the sets themselves (Hart, Sandin and Kauffman).

The standard distance estimator used for a complex or quaternionic quadratic iteration

$f(z) = z^2 + c, \ c \in \pounds$ is: $D \approx \dfrac{|z_n|}{|z'_n|} \ln|z_n|, \ z_n = f^{(n)}(z_0), \ |z'_{n+1}| = 2|z_n||z'_n|$ applying the chain rule to

$f^{(n)}$. This is unchanged for $f_{\theta,c}(z) = e^{-i\theta}z^2 + e^{i\theta}c$, since $|e^{i\theta}| = 1$.

Fig 49: A succession of unbounding volumes iteratively determined using the distance function.

The algorithm iteratively checks the distance to the set using successively smaller unbounding volumes not intersecting the region, to step along the ray closer, but not into the region until the distance to it falls below a given threshold. A calculation of the tangent plane is then made, either by differentiating to get a normal, or by approximating a tangent plane using neighbouring points 'on' the surface. The shading of the point projected onto the screen plane is then coloured according to the lighting and the orientation of the tangent plane.
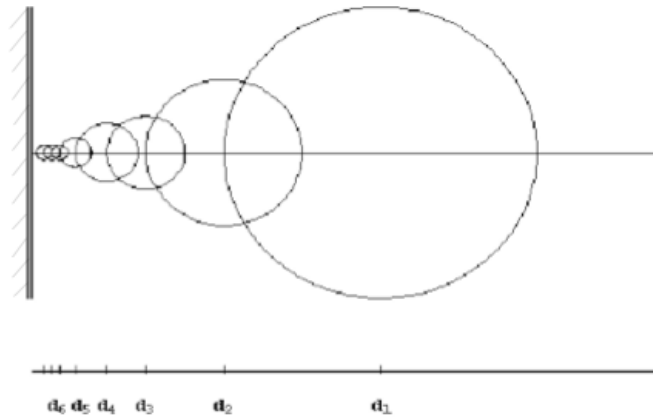
To calculate a normal, a variety of methods can be used. A cross product of vectors to neighbouring points, finding the direction of the point *z* a fixed distance from z_0 on the set whose distance estimation is maximal, finding the direction of maximal attraction, or using a gradient, for example calculated by picking six neighbouring points $N_x = d(x + \varepsilon, y, z) - d(x - \varepsilon, y, z)$ and the same for *y* and *z*, or by directly differentiating the iterative function defining the region.
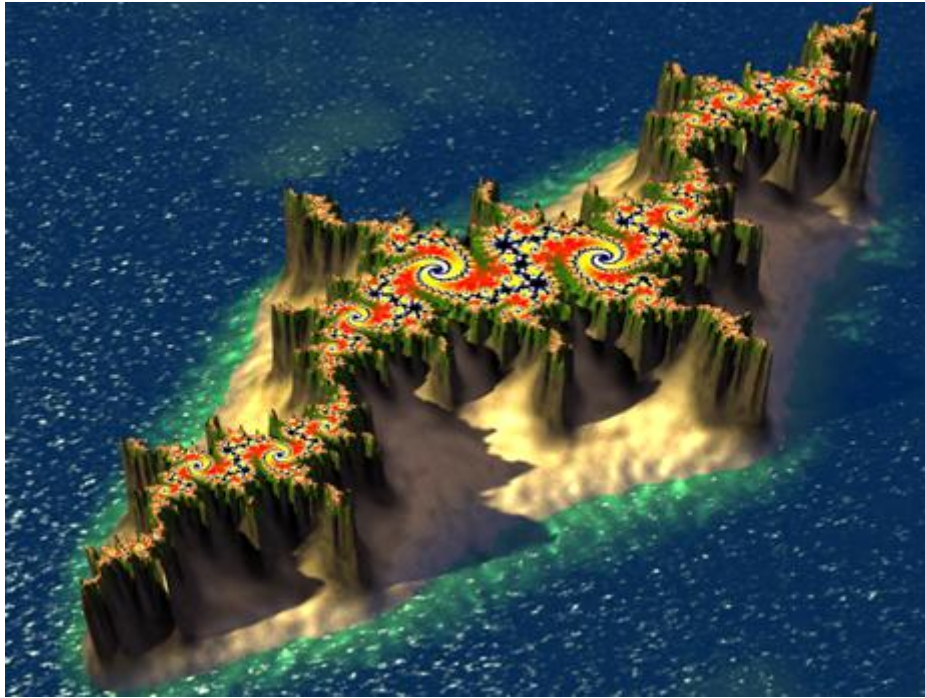
Fig 50: A Julia Island synthesized using the free cross-platform ray-tracing package MegaPOV.

The discrimination radius used to determine how closely neighbouring points on the screen are computed can be made a power law function of distance from the observation point or 'camera', $\Gamma(d) = \alpha d^{\delta}$, so that more distant parts of the image are computed in similar relative precision to nearby parts – a process called 'clarity'.

Bicomplex Numbers
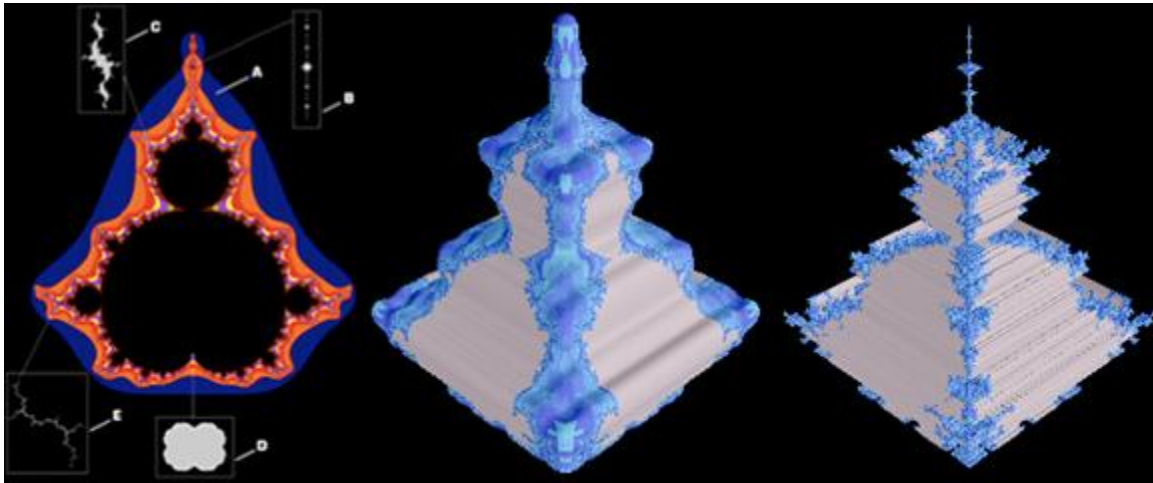
Fig 51: Level sets of the Mandelbrot set (left) correspond (centre, right gray) to product factors of the tetrabrot, for various values of ε.

Bicomplex numbers (Rochon) are defined a little differently from the quaternions:

$$T = \{z = a + bi + ci + dk,\ i^2 = j^2 - 1,\ k^2 = 1,\ ij = ji = k,\ jk = kj = -i,\ ki = ik = -j\}$$

Like the quaternions, bicomplex numbers can be expressed in terms of a pair of complex numbers:

$$z = a + bi + ci + dk = a + bi + (c + di)j = z_1 + z_2 j$$

One can define a generalized Mandelbrot set in *T* in the same way as the complex numbers:

$$M_2 = \{c \in T : f_c^{(n)}(0) \nrightarrow \infty, \, f_c(w) = w^2 + c\}$$

The so-called tetrabrot is then defined as the cross-section of this in $\square^3$

$$\tau = \{c = (p, q, r, 0) \in T : f_c^{(n)}(0) \nrightarrow \infty, \, f_c(w) = w^2 + c\}$$

This set can then be portrayed by colouring the external level sets on the surface of the tetrabrot level set at distance ε surrounding the actual fractal. As ε is reduced, the fractal details of the 3D structure emerge, as shown in fig 3.

T is a commutative unitary ring, but it is not a division ring like the quaternions, so it is not capable of developing a full suite of functions.

The Mandelbulb and Spherical Polar Iterations

Fig 52: Three views of the degree 8 Mandelbulb.

A new development in 2009 driving the compilation of this appendix has been the extending the basic rules of the quadratic Mandelbrot set in 2D polar coordinates to 3D spherical polars.

The iteration $f_c(z) = z^n + c$ in polar coordinates takes the form:

$$x = r\cos(\theta) \leftarrow r^n \cos(n\theta) + c_r, \, y = r\sin(\theta) \leftarrow r^n \sin(n\theta) + c_i$$

This can be readily generalized to the 3D mapping $g_n : \square^3 \rightarrow \square^3$:

$$x = \rho\cos(\theta)\sin(\phi) \leftarrow \rho^n \cos(n\theta)\sin(n\phi) + c_x$$

$$y = \rho\cos(\theta)\sin(\phi) \leftarrow \rho^n \sin(n\theta)\sin(n\phi) + c_y$$

$$z = \rho\cos(\phi) \leftarrow \rho^n \cos(n\phi) + c_z$$

Ray tracing the Mandelbulb in the above figures requires using the distance formula to iteratively differentiate the above function: $dz' = nz^{n-1}$ to produce a Jacobian matrix capable of determining the tangent plane.

$$dz_x = nr^{n-1}r_{dz} \sin\left(\phi_{dz} + (n-1)\phi\right)\cos\left(\theta_{dz} + (n-1)\theta\right) + 1$$

$$dz_y = nr^{n-1}r_{dz} \sin\left(\phi_{dz} + (n-1)\phi\right)\sin\left(\theta_{dz} + (n-1)\theta\right)$$

$$dz_z = nr^{n-1}r_{dz} \cos\left(\phi_{dz} + (n-1)\phi\right)$$

Prespacetime Journal | March 2012 | Vol. 3 | Issue 3 | pp. 254-273
King, C., *Exploding the Dark Heart of Chaos: Part III*

272

Although spherical polar coordinates do not form a number system, and indeed there is no division ring over the reals except for the complex numbers and quaternions, the above iteration at least is well-defined for a variety of integer powers, and the 3D set $Mb = \{(x,y,z) \in \mathbb{R}^3 : g_n^{(k)}(0) \not\to \infty\}$ forms a 3D fractal set similar to the 2D complex Mandelbrot set, particularly for larger *n* in the range of 6 and above.

Just as the complex iteration has odd symmetry for even powers and even symmetry for odd powers, corresponding to (*n*-1)-fold rotational symmetry, as noted in [4.2] and fig 14, the Mandelbulb displays the same symmetry types in both the ϕ and θ dimensions.
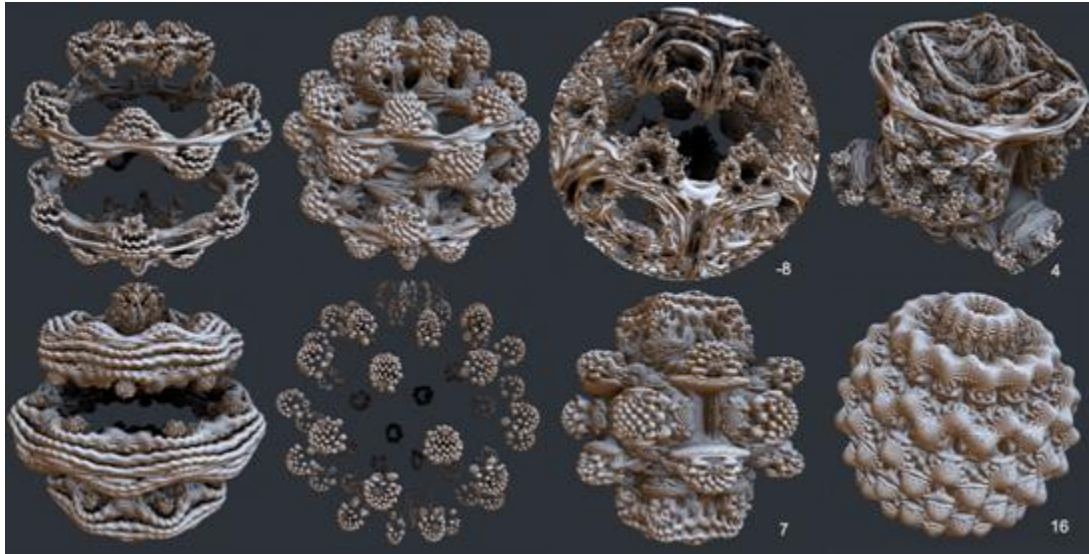
Fig 5: (Left) Four degree 8 Julia sets of the Mandelbulb iteration. (Right) Mandelbulbs of degree -8, 4, 7 and 16. Even degrees have odd symmetry and odd degrees even (compare the degree 7 and 8 side views in figs 4 and 5).

Bibliography:
1. Barnsley M. (1988) *Fractals Everywhere* Academic Press, New York.
2. Brown D, Halstead M (2007) *Super-attracting cycles for the cosine-root family* Chaos, Solitons and Fractals 31 1191-1202.
3. Dang Y, Kauffman L, Sandin D Hypercomplex *Iterations, Distance Estimation and Higher Dimensional Fractals* http://www.evl.uic.edu/hypercomplex/html/book/book.pdf
4. Devaney R.L. (1986) *An Introduction to Chaotic Dynamical Systems* Benjamin/Cummings, Menlo Park.
5. Douady A, Hubbard J. (1985) *On the dynamics of polynomial-like mappings* Ann Sci Ecole Norm Sup 18, 287-343.
6. Durkin M. (1998) *Observations on the dynamics of the complex cosine-root family* J. Differenc Equat Appl 4 215-28.
7. Epstein A., Yampolsky, M. (1996) *Geometry of the Cubic Connectedness Locus I: Intertwining Surgery* arXivMath/9608213v1
8. Halayka S (2009) Some visually interesting non-standard quaternion fractal sets Chaos, Solitons and Fractals 41 2842–2846
9. Griffin C, Joshi G (1992) Octonionic Julia sets Chaos, Solitons & Fractals 2/1 11-24
10. Griffin C, Joshi G (1993) Transition Points in Octonionic Julia Sets Chaos, Solitons & Fractals 3/1 67-88
11. Hart J C, Sandin D, Kauffman L (1989) *Ray Tracing Deterministic 3-D Fractals* Computer Graphics, 23/ 3 289-296
12. Milnor, John W. (1999). *Dynamics in one complex variable*. Vieweg, Wiesbaden, Germany. ISBN 3-528-13130-6.
13. Pastor G, Romera M, Alvarez G, Montoya F (2002) *Operating with external arguments in the Mandelbrot set antenna* Physica D 171 52–71
14. Romera M, Pastor G, Alvarez G, Montoya F (2006) *External arguments in the multiple-spiral medallions of the Mandelbrot set* Computers & Graphics 30 460-469
15. Peitgen H.O. & Richter P.H., (1986), *The Beauty of Fractals* Springer-Verlag, Berlin. DC
16. Peitgen H.O. et.al. (1988) *The Science of Fractal Images* New York ; Berlin : Springer-Verlag
17. Peitgen H.O., Jurgens H., Saupe D. (2004) *Chaos and Fractals: New Frontiers of Science* New York: Springer.

18. Riemann B (1859) *On the Number of Prime Numbers less than a Given Quantity.*
    http://www.maths.tcd.ie/pub/HistMath/People/Riemann/Zeta/EZeta.pdf
19. Rochon, D. (2001) *Dynamique bicomplexe et theoreme de Bloch pour fonctions hyperholomorphes*, Doctoral
    Thesis, Universite de Montreal.
20. Schröder M. (1993) *Fractals, Chaos and Power Laws* ISBN 0-7167-2136-8.
21. Shishikura M. (1994) *The Boundary of the Mandelbrot Set has Hausdorff Dimension Two* Astérisque, 222/7 389-
    405.
22. Tan Lei (1990) *Similarity between the Mandelbrot set and Julia Sets*, Communications in Math. Phys. 134, 587-
    617.
23. Woon S (1998) *Fractals of the Julia and Mandelbrot sets of the Riemann Zeta Function* arXiv:chao-
    dyn/9812031v1

Internet Links:

MegaPOV http://megapov.inetart.net/download.html
Fractal Domains http://www.fractaldomains.com/download.html
Adobe Pixel Bender http://labs.adobe.com/downloads/pixelbender.html
Tom Beddard's Blog http://www.subblue.com/blog
Mandelbulb Skytopia Site http://www.skytopia.com/project/fractal/mandelbulb.html
Quarternionic Fractal Explorer http://www.theory.org/software/qfe/
3D Fractals Bicomplex Mandelbrot http://www.3dfractals.com/
Buddhabrot Movies http://www.superliminal.com/fractals/bbrot/bbrot.htm
Mu-Ency Mandelbrot Encyclopedia http://www.mrob.com/pub/muency.html